



GNITED MINDS
Journals

*Journal of Advances in
Science and Technology*

*Vol. IV, Issue No. VIII,
February-2013, ISSN 2230-
9659*

A STUDY ON PHOTO-CATALYTIC DEGRADATION OF METAL OXIDES

AN
INTERNATIONALLY
INDEXED PEER
REVIEWED &
REFEREED JOURNAL

A Study on Photo-Catalytic Degradation of Metal Oxides

Muralidhara K¹ Dr. Prabhunath Misra²

¹Research Scholar

²Prof. of Physics, Bundelkhand University, Jhansi, UP

Abstract – The research worked on tetragonal copper ferrite (CuFe_2O_4) nano-fibers were fabricated by electro-spinning method using a solution that contained poly(vinyl pyrrolidone) (PVP) and Cu and Fe nitrates as alternative metal sources. The as-spun and calcined CuFe_2O_4 /PVP composite samples were characterized by TG-DTA, X-ray diffraction, FT-IR, and SEM, respectively. After calcination of the as-spun CuFe_2O_4 /PVP composite nano-fibers (fiber size of 89 ± 12 nm in diameter) at 500°C in air for 2 h, CuFe_2O_4 nanofibers of 66 ± 13 nm in diameter having well-developed tetragonal structure were successfully obtained. The crystal structure and morphology of the nano-fibers were influenced by the calcination temperature.

INTRODUCTION

The magnetic properties of the Fe oxides have been extensively studied; in particular, the enhancing magnetic recording properties of magnetic and maghemite for nanostructure materials, or the use of the latter in Fe_2O_3 - SiO_2 composite materials having magneto-optical properties. Most physico-chemical studies are centered in the alpha (corundum structure with a distorted hexagonal anion closed – packed) and gamma (cubic inverse spinel) phases. Size stability of the polymorphs has been studied but there is still a lack of consensus in a significant number of issues; particularly related to the existence of nano-particles with alpha structure.

Chemical properties seem also enhanced by the nanostructure but again a critical role of oxygen vacancies and hydroxyl radicals is noticed. There also been also a lot of work concerning ZnO-based mixed oxides mostly by doping with Mg, Mn and Cd in order to modulate the band gap of the oxide. Fe and O form a number of phases, e.g., FeO (wustite); Fe_3O_4 (magnetite), Fe_2O_3 (hematite), Fe_2O_3 (maghemite). The latter phase is synthetic while remaining oxides occur in nature.

The phase composition of the obtained materials was characterized by XRD, Mossbauer spectroscopy, DSC and TPR analysis. Their catalytic properties were tested in total oxidation of toluene and methanol decomposition to CO and hydrogen. The composite catalysts both with and without pre-reduction were active for DME SR when the pre-reduced catalyst exhibited higher initial activity, but longer activation

process was observed for the composite catalyst without pre-reduction.

The synthesis conditions were systematically studied using statistical design (Box– Behnken Program) and the optimum conditions were determined. The results revealed that single phase of cubic copper ferrite powders can be obtained at different temperatures from 100 to 200°C for times from 12 to 36 h with pH values 8–12.

The crystallite size of the produced powders was in the range between 24.6 and 51.5 nm. The produced copper ferrite powders were appeared as a homogeneous pseudo-cubic-like structure. A high saturation magnetization (M_s 83.7 emu/g) was achieved at hydrothermal temperature 200°C for 24 h and pH 8. Photo-catalytic degradation of the methylene blue dye using copper ferrite powders produced at different conditions was investigated. A good catalytic efficiency was 95.9% at hydrothermal temperature 200°C for hydrothermal time 24 h at pH 12 due to high surface area ($118.4\text{ m}^2/\text{g}$).

Magnetic species was synthesized in a 100 mL Teflon-lined stainless steel autoclave at 180°C for 10 h. The synthesized species was characterized by powder X-ray diffraction, transmission electron microscopy, scanning electronic microscopy, Fourier-transform infrared spectroscopy, X-ray photoelectron spectroscopy and vibrating sample magnetometry at room temperature.

The results showed that the synthesized species was nickel ferrite nano-particles with diameters of

approximately 10 nm. The nano-particles exhibited a photo-Fenton catalytic feature for the degradation of rhodamine B in the presence of oxalic acid. The effects of pH, oxalic acid concentration, and dosage of the catalyst, on the degradation rates of the dyes were examined.

Reactive Red 198 (RR198) and Reactive Red 120 (RR120) were used as dye models. The characteristics of CF nano-particle were studied using Fourier transform infrared (FTIR) and scanning electron microscopy (SEM). UV-Vis and ion chromatography (IC) analyses were employed to study of dye degradation. The effect of operational parameters on dye degradation such as CF nano-particle dosage, pH, dye concentration and salt (inorganic anions) was studied. Formate, acetate and oxalate anions were detected as dominant aliphatic intermediates.

Based on the above results, the oxidations of alcohols were considered to proceed as follows: alcohols are oxidized with oxoammonium moieties on silica and ferrite surface, which were formed by the reaction of surface TEMPO moieties with copper(II) salts, and oxoammonium moieties on the surface itself are reduced to the corresponding hydroxylamine moieties after the oxidation. Then the hydroxylamine moieties are oxidized with copper(II) salts to regenerate TEMPO moieties on the surface. For example, in the case of the oxidation of benzyl alcohol, Silica-TEMPO was recycled about 45 times. Silica-TEMPO and Ferrite-TEMPO were readily recovered from reaction mixture by centrifugation.

REVIEW OF RELATED LITERATURE

Morales *et al.* synthesized manganese iron or nickel mixed oxide catalysts (MnFe or MnNi, respectively). A detailed description of the bulk and surface structure of each system was achieved by means of measurements of specific surface area, XRD, XPS, FT-IR, and Mossbauer spectroscopies. The characterisation results show that MnNi catalysts are formed as NiMnO₃ and Ni₆MnO₈ mixed oxides besides a little amount of Mn₂O₃.

In contrast, MnFe catalysts consist of an oxide mixture (Fe₂O₃, Mn₂O₃ and Mn₅O₈) forming incipiently a solid solution. The catalytic activity was evaluated in the combustion of propane and ethanol, selected as model volatile organic compounds. Luca and coworkers used the tar reforming catalytic activity of iron and nickel based catalyst supported on alkaline-earth oxides CaO, MgO and calcined dolomite solid solution investigated in a fixed bed reactor operating at temperatures ranging from 650 to 850 °C; Toluene and 1-methyl naphthalene were used as model compounds for tar generated during bio-mass gasification.

Mostafa *et al.* synthesized the iron nickel oxide catalysts were prepared using co-precipitation procedure and studied for the conversion of synthesis gas to light olefins. In particular, the effects of a range

of preparation variables such as [Fe]/[Ni] molar ratios of the precipitation solution, precipitate aging times, calcination conditions, different supports and loading of optimum support on the structure of catalysts and their catalytic performance for the tested reaction were investigated. It was found that the catalyst containing 40%Fe/60%Ni/40wt%Al₂O₃, which was aged for 180 min and calcined at 600 °C for 6 h was the optimum modified catalyst.

Guan *et al.* prepared the calcined scallop shell (CS) applied for the adsorption and decomposition of biomass -derived tar. In this study, steam reforming of tar derived from pruned apple branch over CS was investigated in a fixed bed at 650 °C. It was found that CS had good activity for the steam reforming of tar to produce synthesis gas (syngas), and was able to be recycled. To promote the gas production efficiency, iron or nickel was supported on the CS, and used for the reforming of tar. The effect of heating rate on the gas production rate was investigated, and it was found that reduced iron or nickel supported CS showed better activities under the condition of rapid heating. Iron or nickel based catalyst in its oxide state was also investigated for the reforming of tar.

Huang *et al.* showed the iron-doped nickel oxide films application as oxygen evolution catalysts in the photo-electrochemical production of hydrogen from solar energy. The effects of processing parameters on the film properties, such as over-potential, composition, surface morphology and preferred orientation, were investigated. The electrochemical experiment, structural and compositional measurements indicate that the relative lower substrate temperature, higher RF power, higher working pressure and oxygen content are necessary to gain lower over-potential.

Rahman and co-workers carried out nickel oxide on alumina aerogel catalysts convert propylene into acrylonitrile through the interaction with nitric oxide (nitrooxidation). For a NiO/Al₂O₃ aerogel catalyst, with Ni:Al ratio 1:1, the activity decreases by about 20% over a 3-h run. Simultaneously, a carbon deposit is observed on the catalyst which results from the cracking of hydrocarbons and from the boudouard reaction of generated carbon monoxide. Addition of water vapor into the feed slows down the deactivation process by promoting the water-gas shift reaction without affecting the activity. Addition of a basic component like magnesia (0.2 Mg : 0.8 Ni) to the NiO/Al₂O₃ aerogel catalyst also enhances the stability by retarding the cracking reactions.

Huang *et al.* studied iron-doped LaNiO₃ catalysts with a perovskite structure prepared via self-combustion and tested in auto-thermal reforming (ATR) of ethanol. Characterizations of temperature-programmed surface reaction (TPSR), X-ray diffraction (XRD), physical N₂ adsorption, and temperature-programmed reduction (TPR) were carried out. The results indicate that LaNiO₃ perovskite structure was successfully formed via self-

combustion. With iron-doping in LaNiO_3 , the perovskite structure still remains, in the form of solid solution $\text{La}(\text{Ni}, \text{Fe})\text{O}_3$, where iron is reducible and the nickel-iron alloy forms after the reduction. In addition, the surface area of the iron-doped samples increased.

Morozova *et al.* discovered the NiO and $\alpha\text{-Fe}_2\text{O}_3$ samples from various backgrounds and used as precursors of the catalysts for CO hydrogenation. The effect of the initial microstructure of oxides on the morphological peculiarities and catalytic properties of the newly formed catalysts was studied using transmission electron microscopy and in situ XRD combined on-line with gas-chromatographic analysis.

Tsoncheva and coworkers found that several SBA-15 type mesoporous silicas, where different means of surfactant removal have been used, have been modified by copper and iron oxide, and tested as catalyst for methanol decomposition. The materials were thoroughly characterized by nitrogen physisorption, X-ray diffraction, Moessbauer spectroscopy and temperature programmed reduction with hydrogen. The different means of template removal results in SBA-15 materials different in mesopore size and degree of microporosity. These parameters have a strong influence on the reductive and catalytic properties of the obtained composite materials.

Natter *et al.* studied cluster models for sites on the {1 1 1} surface of Fe_3O_4 and used to study the strength of bonding of water-gas shift intermediates using density functional theory. Three site models were used, representing an unpromoted catalyst, a catalyst where copper cations substitute for iron cations below the surface and a catalyst where copper cations substitute in the surface. The strengths of bonding of oxygen, carbon dioxide, dissociated water and dissociated formic acid were all observed to decrease by less than 20 kJ mol^{-1} when copper substituted below the surface, but they decreased by $60\text{--}80 \text{ kJ mol}^{-1}$ when copper substituted in the surface of the catalyst.

Tsoncheva and coworkers examined mixed copper and iron modified MCM-41 mesoporous silica with various Cu/Fe ratio characterized by N_2 physisorption, X-ray diffraction (XRD), transmission electron micrographs (TEM), X-ray photoelectron spectroscopy (XPS), moessbauer spectroscopy and temperature programmed reduction with hydrogen. Their catalytic properties in methanol decomposition to CO and H_2 are investigated and compared with that of the corresponding mono-component materials. The catalytic behavior of bi-component materials are discussed based on the nature of the catalytic active sites.

RESEARCH METHODOLOGY

Photo-catalytic activity towards hydrogen generation from water was investigated using a multiport photo-catalytic reactor under visible light illumination with methanol. Three calcination temperatures were selected – 300, 400 and 500 °C. It was found that 10 wt.% Cu/ TiO_2 calcined at 300 °C for 30 min yielded the maximum quantity of hydrogen.

Also, we prepared the novel CuO-SnO_2 nano-composite oxide photo-catalysts. The maximum photo-catalytic activity of the CuO-SnO_2 photo-catalyst was observed to be calcined at 500 °C for 3 h (the molar ratio of Cu to Sn was 1:1) due to the sample with good crystallization and high surface area.

Xu *et al.* showed 1-D mesoporous TiO_2 nanotube (TNT) with large BET surface area and employed for simultaneous photo-catalytic H_2 production and Cu^{2+} removal from water. Cu^{2+} , across a wide concentration range of 8–800 ppm, was removed rapidly from water under irradiation. The removed Cu^{2+} then combined with TNT to produce efficient Cu incorporated TNT (Cu-TNT) photo-catalyst for H_2 production. Average H_2 generation rate recorded across a 4 h reaction was between 15.7 and 40.2 $\text{mmol h}^{-1} \text{ g}^{-1}$ depending on initial Cu^{2+}/Ti ratio in solution, which was optimized at 10 atmosphere.

In addition, reduction process of Cu^{2+} was also a critical factor in governing H_2 evolution. In comparison with P25, its large surface area and 1-D tubular structure endowed TNT with higher photo-catalytic activity in both Cu^{2+} removal and H_2 production.

The research carried out an ultrasound – assisted method for synthesizing nanosized Pt-graphene oxide (GO) – TiO_2 photo-catalyst. The Pt-GO- TiO_2 nano-particles were characterized by diffused reflectance spectroscopy, X-Ray diffraction, N_2 adsorption – desorption measurements, atomic force microscopy and transmission electron microscopy. The intermediate products formed during the degradation of DBS were monitored using electrospray mass spectrometry. The ability of GO to serve as a solid support to anchor platinum particles on GO- TiO_2 is useful in developing new photo-catalysts.

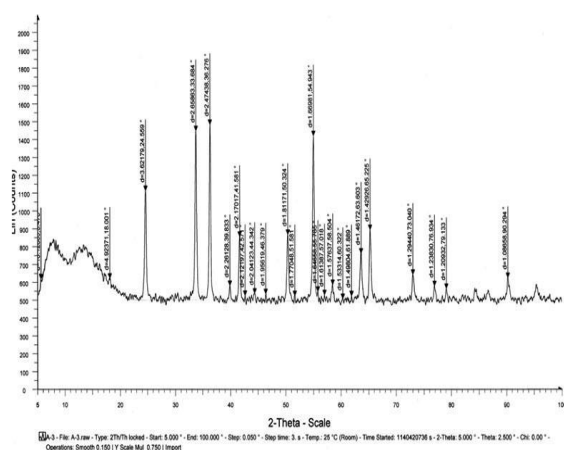
Xu *et al.* studied efficient Cu incorporated TiO_2 (Cu- TiO_2) photo-catalysts for hydrogen generation fabricated by four methods: in situ sol-gel, wet impregnation, chemical reduction of Cu salt, and in situ photo-deposition. Among the four photo-catalysts, the sample that was synthesized by in situ sol-gel method exhibited the highest stability. High efficiency, low cost, good stability are some of the

merits that underline the promising potential of Cu-TiO₂ in photo-catalytic hydrogen generation.

The study discovered floating photo-catalysts based on composites of low density polyethylene (LDPE) containing 30, 68 and 82 wt.% of TiO₂ P₂₅. The floating photo-catalyst can be reused for at least three consecutive times without any significant decrease on the discoloration and total organic carbon removal after each reuse.

Hu and coworkers investigated different p-type Cu₂O powders prepared from electro-deposition and subjected to analysis of their photo-catalytic activity in water reduction. The electrodeposited Cu₂O powders were obtained by scraping the deposited films off the substrate. The coupling was made to avoid back reactions of the photo-induced charges. Appropriate crystalline-texture tuning, as well as charge delocalization promotion, is looked to as the key issue for efficient H₂ generation from water reduction over p-type Cu₂O photocatalysts.

It was found that highly dispersed CuO was introduced into TiO₂ nanotube (TNT) made by hydrothermal method via adsorption– calcination process or wet impregnation process to fabricate CuO incorporated TNT photocatalysts (CuO-TNT) for hydrogen production. This high photo-catalytic activity of CuO - TNT was mainly attributed to the unique 1-D tubular structure, large BET surface area and high dispersion of copper component. Compared to wet impregnation, adsorption–calcination process was superior to produce active photocatalyst, since it was prone to produce photocatalyst with more highly dispersed CuO.



DATA ANALYSIS

The 110 K T_c onset progressively decreases to about 90 K as a function of annealing time and/or temperature when the samples are treated under vacuum or under nitrogen gas, and increases again after further thermal treatments under oxygen even at a temperature as low as 100°C, reaching 110 K when annealed at 250-300°C. In contrast, the 85 K

transition is slightly modified under the same conditions. Nanocrystalline CuZnO thin films were prepared on p-type Si (1 0 0) substrates by spin coating from a CuO solution mixed with Zn of 0.8.0 at %.

When the Zn doping concentration was above 4.0 at % the crystalline quality and preferential orientation of the thin film weakened in turn. The XRD and FT-IR results showed single phase CuZnO for the lower (at % ≤ 6.0) Zn Concentration. The works showed that the structural and optical properties of CuO films doped with Zn can be improved and the 4.0 at % Zn-doped CuO thin films have the best crystallization quality and the strongest emission ability. We checked superconducting YBa₂(Cu_{1-x}Cr_x)₄O₈ (x=0.01; 0.03; 0.05; 0.01; 0.20) oxides synthesized by the aqueous sol-gel method. Effects of chromium substitutions on the properties of compounds were studied by resistively measurements, X-ray powder diffraction, infrared spectroscopy, electron microscopy and elemental analysis. The point defect chemistry approach, which explains the change of T_c by substituting chromium for copper in the YBa₂Cu₄O₈ superconductor, is presented.

It was analyzed that in the diffusion mechanism of iron impurities in bulk YBa₂Cu₃O₇ (YBaCuO) superconductor prepared by standard solid state reaction method and its effect on lattice structure under different magnetic field have been examined. The effects of different magnetic field intensities on crystal structure of iron diffused samples have been investigated by quantitative Energy Dispersive X-Ray Fluorescence (EDXRF) and X-Ray Diffraction (XRD) techniques.

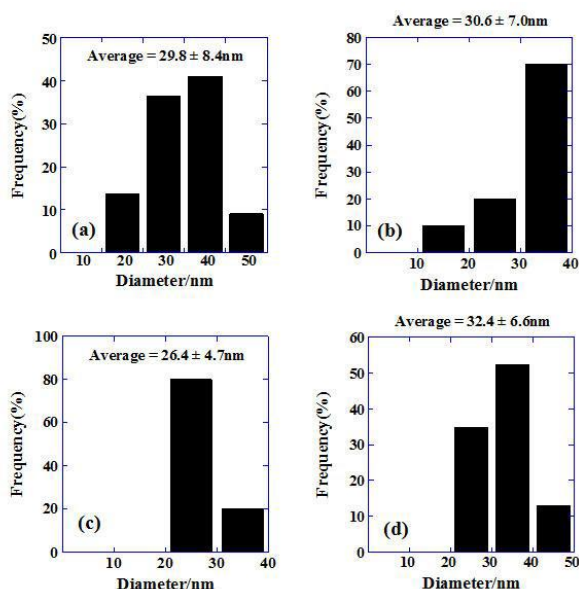
It was noticed that the epitaxial growth of Fe-based superconductors such as CO-doped SrFe₂As₂ (SrFe₂As₂: Co) still has insufficient properties for a device application because they have rough surfaces and are decomposed by reactions with water vapor in an ambient atmosphere. These films also have atomically – flat surfaces with step-and – terrace structures and exhibit chemical stability against exposure to water vapor. It was noticed that pressure of superconducting transition temperature (T_c) FeSr₂YCu₂O₈ samples were synthesized by solid-state reaction with multiple annealing process.

Ekino *et al.* synthesized tunnel break junction method adopted to study polycrystalline samples of iron oxypnictide superconductor NdFeAs (O_{0.9} F_{0.1}) with T_c=48K. Measurements were carried out at 4.2K. Break –junction (BJ) conductance versus voltage curves showed gap-edge peaks with the peak to peak distances at 4.2 K where the superconducting energy gap $\epsilon > 0$ is the elementary change. This ratio implies strong – coupling superconductivity in the framework of Bardeen- Copper – Schrieffer theory, being, how very much, smaller than that for high T_c copper oxides.

These synthesis temperatures have been established by optimization. The partial substitution of Se by Te leads to an enhancement of T_c to 13K. The non-superconducting telluride $\text{Fe}_{1.09}\text{Te}$ exhibits a metal-insulator phase transition at 82K. Substitution studies of this telluride system by S and Si have in addition been carried out to investigate if chemical pressure induces superconductivity. It was reported that the detailed measurements of the temperature dependence of the lower critical field H_{c1} of the FeAs – based superconductor $\text{SmFeAsO}_{0.9}\text{F}_{0.1}$ (Sm-1111) and $\text{Ba}_{0.6}\text{K}_{0.4}\text{Fe}_2\text{As}_2$ (Bak-122) by global and local magnetization measurements.

Excellent fitting to the data can be reached with two s-wave superconducting gaps. Comparison of the absolute values of $H_{c1}(0)$ between Sm-1111 and Bak-122 shows a relatively large super-fluid density for the latter.

It showed the upper critical fields (H_{c2}) of the single crystals (Sr, Na) Fe_2As_2 and $\text{Ba}_{0.55}\text{K}_{0.45}\text{Fe}_2\text{As}_2$ determined by means of measuring the electrical resistivity, using the facilities of pulsed magnetic field at Los Alamos such a difference mainly results from the multi-band effect, which might be modified via doping. The research carried out novel superconducting characteristics and unusual normal state properties in iron based prictide superconductors by mean of studies in REFeAsO_{1-y} (RE=La, Pr, Nd) and $\text{Ba}_{0.6}\text{K}_{0.4}\text{Fe}_2\text{As}_2$ ^{57}Fe NMR and ^{75}As NQR/NMR. Fe_2As_2 .



It was discovered that the magnetic hysteresis loops of $\text{YBa}_2\text{Cu}_3\text{O}_y$, $\text{Ln}_{1+x}\text{Ba}_{2-x}\text{Cu}_3\text{O}_y$ (Ln=Sm, Nd) and $\text{YBa}_2(\text{Cu}_{1-x}\text{Fe}_x)_3\text{O}_y$ systems measured by a superconducting quantum interference device (SQUID), magnetometer, and the relationship between the microscopic structure and effectiveness of pinning centres for the flux lines.

Selective adsorption and separation of Chromium (VI) on the magnetic iron – nickel oxide form waste nickel liquid used. A new composite adsorbent, iron oxide coated zeolite (IOCZ), was characterized and employed for the removal of Cu (II) from aqueous solution using fixed bed column. Scanning electron microscope (SEM), FTIR, X-ray diffraction spectrum (XRD) and BET analyses were used to study the surface properties of the coated layer.

The Thomas model was found suitable for the description of breakthrough curve at all experimental conditions, while Adams- Bohart model was only for an initial part of dynamic behavior of the IOCZ column. The theoretical breakthrough curve profile in the dynamic process. The saturated column was regenerated by 1 mol^{-1} hydrogen chloride solution and IOCZ could be reused in Cu (II) removal.

CONCLUSION

Modeling the sorption of metal ions from aqueous solution by iron based adsorbents were studied. The possibility of using iron-based adsorbents (i.e. akaganéite or goethite) to remove heavy metal ions from aqueous solutions. The removal efficiency of the packed-bed column was examined and compared. Typical adsorption models were discussed and the bed depth-service time equation has been applied to the sorption results in order to model the column operation.

Hexavalent chromium is a well – known highly toxic metal, considered a priority pollutant. Industrial sources of Cr (VI) include leather training, cooling tower blow-down, plating, electroplating, anodizing baths, rinse waters, etc. The most common method applied for chromate control is reduction of Cr (VI) to its trivalent form in sold (pH) and subsequent hydroxide precipitation of Cr (III) by increasing the pH to 9.0-10.0 using lime. After an overview of chromium contamination is provided, more than 300 papers on chromium remediation using adsorption are discussed to provide recent information about the most widely used adsorbents applied for chromium remediation.

The adsorption behaviors of lanthanum (III) from an aqueous chloride medium, using iron oxide loaded calcium alginate beads were studied using equilibrium batch and column flow techniques. The effect of pH, contents of loaded iron oxide, ionic strength, adsorbent dose, contact time, and temperature on adsorption capacity of the magnetic beads was investigated. The Langmuir adsorption isotherm models were used for the description of the adsorption process. Furthermore, column breakthrough curves were obtained and the La (III)

loaded magnetic beads were regenerated using 0.05 mol/L CaCl_2 solution.

The adsorption features of multiwall carbon nanotubes (MWCNTs) with the magnetic properties of iron oxides have been combined in a composite to produce a magnetic adsorbent. Composites of MWCNT/nano-iron oxide were prepared, and were characterized by X-ray diffraction (XRD), field emission scanning electron microscope (FESEM) and Fourier transform infrared spectroscopy (FTIR). The composites have demonstrated a superior adsorption capability to that of activated carbon. The results also show that the adsorptions of Cr (III) on the composites is strongly dependent on contact time.

REFERENCES

- J. Z. Huang Z. Xu, H. L. Li, G. H. Kang, W. J. Wang, *Transactions of Non Ferrous Metal of China*, **16** (2006) 1301-1306.
- M. Rahman, R. J. Wiley and S. J. Teichner, *Appl. Catalysis*, **36** (1988) 209-220.
- L. Huang, F. Zhang, N. Wang, R. Chen, A.T. Hsu, *Int. J. of Hydrogen Energy*, **36** (2012) 1272-1279.
- O. S. Morozova, O. V. Krylov, G. N. Kryukova and L. M. Plyasova, *Int. J. of Hydrogen Energy*, **33** (1997) 323-334.
- T. Tsoncheva, J. Rosenholm, M. Linden, L. Ivanova and C. Minchev, *Appl. Catalysis A: General*, **318** (2007) 234-243.
- R. M. V. Natter, J. S. Coleman and C. R. F. Lund, *J. of Molecular Catalysis Chemical*, **311** (2009) 17-22.
- C. H. Zhang, Y. Yang, B. T. Teng, T. Z. Li, H. Y. Zheng, H. W. Xiang and Y. M. Li, *J. of Catalysis*, **237** (2006) 405-415.
- S. Caudo, G. Centi, C. Genovese and S. Perathoner, *Appl. Catalysis B: Environmental*, **70** (2007) 437-446.
- N.Tsubokawa, T.Kimoto and T.Endo, *Journal of molecular catalysis A: Chemical*, **101** (1995) 45-50
- L. Andronic, L. Isac and A. Duta, *J. of Photochem. And Photobiology A: Chem*, (2011) 30-37.
- N.Aman, T. Mishra, J. Hait and R.K. Jana, *J. of Hazardous Mat.*, **186** (2011).
- L.S. Yoong, Chong and B.K. Dutta, *Energy*, **34** (2009) 1652-1661.
- H.I. Xia, H.S. Zhuang, T. Zhang and D.C. Xiao, *J. of Environmental Science*, **19** (2007) 1141-1145.
- S. Xu, J. Ng, A. J. Du, J. Liu and D.D. Sun., *International J. of Hydrogen Energy*, **36** (2011) 6538-6545.